Surface-Confined Atom Transfer Radical Polymerization from Sacrificial Mesoporous Silica Nanospheres for Preparing Mesoporous Polymer/Carbon Nanospheres with Faithful Shape Replication: Functional Mesoporous Materials

*Sanjib Banerjee, Tapas K. Paira, Atanu Kotal, and Tarun K. Mandal**

A facile approach for the preparation of mesoporous polymer nanospheres (MPN) and mesoporous carbon nanospheres (MCN) with complete shape retention based on surface-confined atom transfer radical polymerization of various methacrylate monomers from in situ generated initiator-modified hard silica nanospheres template is developed. This approach yields mesoporous silica-polymer hybrid nanospheres (MSPN) with mesopores that are uniformly filled with covalently attached well-defined poly(methacrylate)s. The silica frameworks are subsequently etched, resulting in MPN. Pyrolysis of MSPN and subsequent removal of silica template resulted in the production of MCN. They retain the size, shape, and mesoporous ordering of the silica template nanospheres. Gel permeation chromatography analysis of the silica free polymers reveals that they have controlled molecular weights and low polydispersities (PDIs). Kinetics studies reveal that the molecular weight of the grafted polymer increases linearly with time, maintaining low PDIs, indicating the living nature of the polymerization. The mesoporous polymer material is found to have low dielectric constant, which paves the way for their use as low-dielectric constant materials in microelectronics. This approach allows fabrication of functional MPN using functional comonomers, which are successfully used for the synthesis of "clickable" mesoporous polymer nanospheres, removal of ionic contaminates through anion exchange, and glucose sensing.

1. Introduction

Over the last few years, the interest in ordered mesoporous materials (pore size: 2–50 nm), has grown exponentially because these materials have an extremely high surface area and large pore volume. This makes the materials useful for applications in separation, adsorption, chemical sensor, catalysis and synthesis of host–guest functional material.[1,2] Also, they are highly desirable for optical sensor applications,[3] energy storage and information processing[4] and as Magnetic Resonance Imaging (MRI) contrast agents.[5] Among them, mesoporous polymer (MP) materials has potential use in electronics,[6] controlled release[7] and heterogeneous catalysis.[8] Mesoporous carbon (MC) materials are also used as an adsorbent of bio and organic molecules,[9] catalyst supports,[10] component of fuel cells[11] and component of Li ion batteries.[12]

Because of such diverse applicability, to date, several synthetic strategies have been developed to prepare mesoporous materials. For example, MP materials were fabricated by free-radical polymerization using triblock copolymer Pluronic 25R4 as soft-template;[13] using block copolymer precursor;[14] by templating of liquid crystalline phases.[15] Similar soft-templating approach has also been used to make MP materials by condensation polymerization using resorcinol/formaldehyde and Pluronic F127,[16,17] and oligomeric phenolic resin and Pluronic P123.[18] The later MP materials ultimately converted into MC materials by carbonization where resorcinol/formaldehyde and oligomeric phenolic resin were used as carbon sources, respectively. A template-free approach has also been introduced to make MP materials and ultimately to MC materials by dissolving polyacrylonitrile (PAN) in water/dimethyl sulfoxide (DMSO) mixture[19] and by self-assembly of diblock copolymers.[20] Another important strategy to prepare MP/MC materials is the use of mesoporous silica as a hard template. Wu and Bein was the first to apply this approach for preparing MC by filling MCM-41 with PAN via radical polymerization and subsequent carbonization of the polymer and etching the silica.[21] Johnson et al. reported the synthesis of ordered mesoporous polymer of tunable pore size using colloidal silica as the template.[22] Zhou and his co-workers successfully synthesized mesoporous polymer materials using different synthetic strategies and showed that these could be used as potential materials in gas storage/separation.[23–25] Similarly, Lu et al. synthesized MC by polymerizing acrylonitrile (AN) using mesoporous silica SBA-15 as a

S. Banerjee, T. K. Paira, A. Kotal, Prof. T. K. Mandal
Polymer Science Unit
Indian Association for the Cultivation of Science
Jadavpur, Kolkata 700 032, India
E-mail: psutkm@iacs.res.in

DOI: 10.1002/adfm.201200261

template.[26,27] MC was also synthesized by carbonizing the soybean oil filled SBA-15 at 700 °C followed by silica etching.[28] Recently, Matyjaszewski's group developed strategies for the preparation of MC via surface-confined atom transfer radical polymerization (SC-ATRP) of AN from hard templates such as silica nanoparticles and mesoporous silicas.[27,29–31] There are also some reports of growing polymer chains from mesoporous silica via SC-ATRP[30,32–35] and nitroxide-mediated polymerization.[36] In general, the initiation sites on silica template were created by post functionalization of the hard silica templates. Therefore, the process may yield functionalized silica with poor grafting of initiator into the pores of silica. Also, no one really tried to explore the production of well-ordered MP materials by removing the template from as-synthesized silica-polymer hybrids. Again, almost all of these publications report the production of MP or MC powdery materials, that is, powders with no definite shape. On the other hand, the synthesis of materials with controlled and tunable morphologies is an interesting and growing area in the field of materials science. Especially, the production of materials with definite shape via shape replication is the big challenge. In this context, there are only very few studies that concentrates on the preparation of mesostructured polymer/carbon particles from porous inorganic particles via shape replication. Sozzani et al. first reported successful shape transcription from mesoporous silica to polymeric replica by free-radical polymerization, but the obtained polymers have broad molecular weight distributions (polydispersity index, PDI ≥ 2.04).[37] Therefore, it will be interesting to explore the possibility of synthesizing MP replica nanospheres composed of polymers with controlled molecular weights, well-defined functionalities and low PDIs by SC-ATRP using mesoporous silica nanospheres as the hard template. It would also be interesting to prepare MC of definite shape by such replication technique.

Furthermore, the introduction of specific functionalities into the MP surface is also very important considering its applications in diverse areas, especially in the field of catalysis,[38] sensors[39,40] and removal of non-biodegradable industrial waste.[41] In general, post-synthesis modification technique is the most common method to functionalize the MP by attaching active sites to the pore surface through surface chemical reaction.[38,42] However, the direct-functionalization approach was also reported, where the functionalized organic oligomers were used to produce MP in presence of different templates.[43] The later method would likely produce MPs with more uniform distribution and higher loading of functional groups.[18,44]

Here, we report the synthesis of mesoporous polymer nanospheres (MPN) and mesoporous carbon nanospheres (MCN) with high specific surface areas and large pore volumes that are faithful replicas of mesoporous silica nanospheres (MSN). Using the in situ generated initiator-grafted mesoporous silica nanospheres (MSIN) as sacrificial template, MPN are prepared by template dissolution. A surface-confined atom transfer radical polymerization (SC-ATRP) of various methacrylate monomers is conducted using MSIN to produce mesoporous silica-polymer hybrid nanospheres (MSPN) and subsequent etching of silica template leads to the production of MPN. Pyrolysis of MSPN hybrid and subsequent removal of silica template resulted in the production of MCN. The obtained MPN are found to have low dielectric constant (low-*k*). The synthesis strategy is applied to introduce specific functions into the synthesized MPN by copolymerization of functional monomers with MMA. The resultant functional MPN are used for different applications like formation of triazole functionalized MPN using click chemistry, removal of anionic dye from contaminated water by anion exchange and glucose sensing.

2. Results and Discussion

2.1. In Situ Formation of Initiator (CMPE)-Grafted Mesoporous Silica Nanospheres (MSINs)

MSIN were synthesized by hydrolysis/condensation reaction of TEOS and CMPE-TMS at a basic pH (≈12) in presence of CTAB as the template and subsequently removing the template by an acid extraction (**Scheme 1**).[45] The addition of (chloromethyl) phenylethyl (designated as CMPE) containing trimethoxysilyl group led to the incorporation of chlorine in the MSIN. The FTIR spectrum (Figure S1 in the Supporting Information) of the MSIN reveals bands at 1450, 1513 and 1638 cm^{-1} (phenyl ring stretching vibration); 1415 cm^{-1} (CH_2 of -CH_2Cl group); 707 cm^{-1} (typical benzene-ring stretching, consisting of a polystyrene skeleton); 2934 cm^{-1} (C-H asymmetric stretching vibration); 1087 cm^{-1} (Si-O-Si linkage) of silica network indicating the successful incorporation of CMPE initiator moiety. The XRD pattern (**Figure 1**A) of neat mesoporous silica nanospheres (MSN) featured three reflection peaks: an intense (100) reflection peak at $2\theta = 2.42°$ and two additional peaks at $2\theta = 4.09°$ and $2\theta = 4.73°$ due to reflection from (110) and (200) plane respectively, indicating the presence of channel-like pores arranged in a hexagonal honey comb pattern with a high

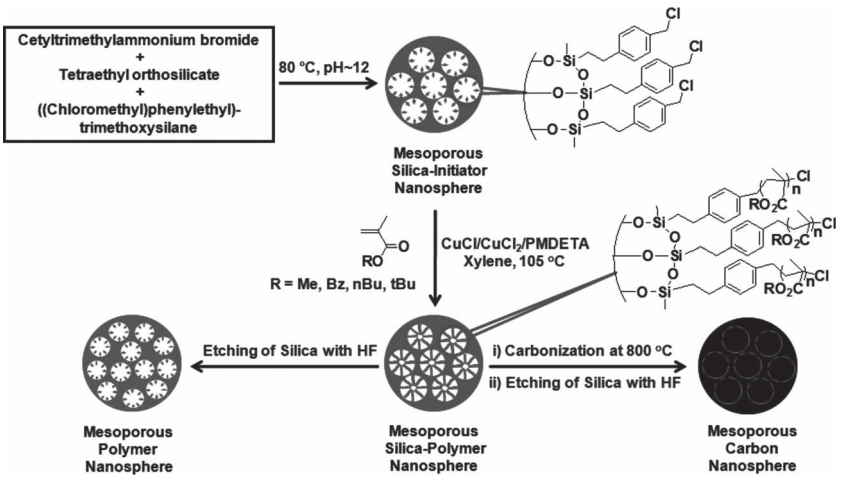

Scheme 1. Schematic illustration of the synthesis of mesoporous silica initiator, silica-polymer hybrid, polymer, and carbon nanospheres.

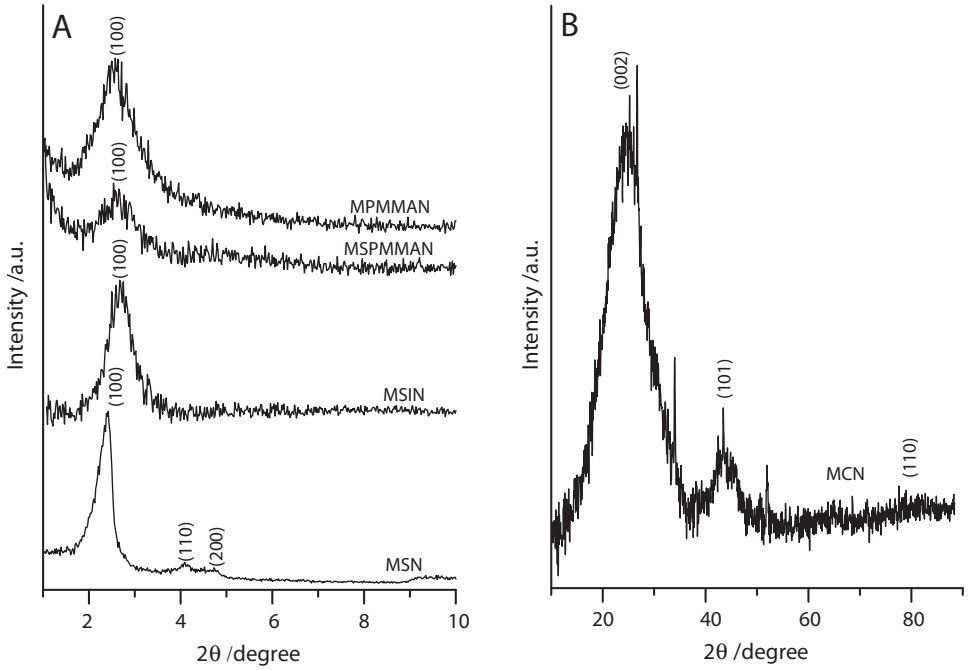

Figure 1. A) Low-angle XRD patterns of different mesoporous nanospheres. B) High-angle XRD pattern of MCN.

degree of regularity.[46] The XRD pattern of MSIN (Figure 1A) displayed an intense (100) reflection peak at $2\theta = 2.75°$ indicating that the arrangement of the cylindrical pores is maintained even after incorporation of CMPE group onto the pores of the MSN.[45] The decrease in the number of reflection peaks in the XRD pattern of MSIN compared to that of MSN might be due to the different ordering of the mesopores, which will be confirmed later by TEM analysis. The N_2 adsorption/desorption analyses of both the MSN and MSIN materials (Figure S2A in the Supporting Information) reveal a characteristic Type IV BET isotherms suggesting the presence of cylindrical mesopores.[45] **Table 1** reveals that specific surface area (S_{BET}) of MSIN (1200 $m^2\ g^{-1}$) is much higher than that of neat MSN (533 $m^2\ g^{-1}$). The BJH analysis of these isotherms for neat MSN and MSIN materials revealed narrow pore size distributions (PSD) (Figure S2B in the Supporting Information) with an average diameter of around 2.20 and 1.99 nm respectively, while the total pore volume are 0.189 and 0.703 cc g^{-1} respectively (see Table 1). This is probably due to the difference in ordering of mesopores in the MSN and MSIN, as evident by TEM images, discussed later in this section. The noticeable weight loss registered in case of neat MSN was 6.7% between 120 °C to 800 °C (Figure S3 in the Supporting Information) is due to elimination of physisorbed water or adsorbed gases. While for the MSIN in the same temperature range, the corresponding weight loss was 28.4% (Figure S3 in the Supporting Information), which is attributable solely to the CMPE moiety as silica component remains thermally stable at that temperature range. The initiator grafting density (G_I) of MSIN was found to be 0.9 molecule nm^{-2}, calculated based on the equation reported elsewhere (see Supporting Information).[32] FESEM images (**Figure 2**) showed that both the neat MSN and MSIN have spherical geometry with typical size ranges of 222–399 and 166-381 nm respectively. The TEM images (**Figure 3**) of the MSN and MSIN also

Table 1. Characterizations of different mesoporous nanospheres.

Sample	D_{SEM}[a)] [nm]	D_{TEM}[b)] [nm]	D_h[c)] [nm]	S_{BET} [$m^2\ g^{-1}$]	Total pore volume [cc g^{-1}]	Pore diameter [nm]
MSN	222-399	368-430	357	533	0.189	2.20
MSIN	166-381	228-385	339	1200	0.703	1.99
MSPMMAN	172-340	140-312	262	90	0.048	–[d)]
MPMMAN	156-299	89-146	191	520	0.190	1.62
MCN	153-302	133-327	1620	658	0.540	5.66

[a)]Diameter measured from FESEM; [b)]Diameter measured from TEM; [c)]Hydrodynamic diameter measured from DLS; [d)]Mesopores were not accessible to nitrogen adsorbate.

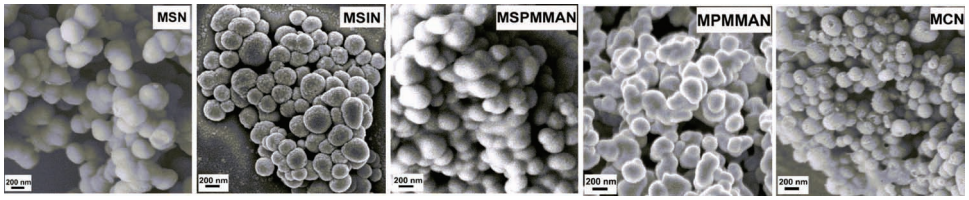

Figure 2. FESEM images of different mesoporous nanospheres.

reveals spherical particles and their sizes correlate well with that obtained from FESEM (Table 1). The high magnification TEM image (Figure 3) revealed that the pores are uniformly aligned along the long axes in the case of MSN, whereas in the case of MSIN, the pores are randomly oriented. FESEM-energy dispersive X-ray (EDX) analysis of selected area reveals absence of any carbon for MSN sample (Figure S4 in the Supporting Information). Only O and Si are present in the MSN in an atom% ratio of 65:35. The FESEM-EDX spectrum clearly reveals the presence of C, Si and O in MSIN in the ratio of 2.4:53.1:44.5. The presence of carbon indicates the successful grafting of organic moiety CMPE into the mesopores of MSIN.

These MSN and MSIN samples' suspensions were examined via dynamic light scattering (DLS) to provide further support that they are not aggregated or coalesced in suspension. The lognormal distributions of the sizes of the nanospheres indicate that the hydrodynamic diameters (D_h) of the MSN and MSIN are 357 and 339 nm respectively (Figure S5A in the Supporting Information and Table 1). The D_h values are correlated well with the diameters measured from FESEM and TEM (see Table 1).

2.2. Surface-Confined ATRP (SC-ATRP) of Various Methacrylates from MSIN Templates

(Chloromethyl)phenyl (benzyl chloride) unit was previously used as the ATRP initiator to graft polymers onto the outer surface of silica.[47,48] However, we used an in situ co-condensation strategy for grafting of the ATRP initiator (CMPE) moiety exclusively to the inner walls of mesopores of MSN. Therefore, as expected, polymer growth is confined to the surface of the mesopores of MSIN. The SC-ATRP of methacrylate monomers was always performed in the presence of a deactivator ($CuCl_2$) and CuCl/PMDETA as catalyst. In case of surface initiated ATRP, the amount of deactivator produced by the persistent radical effect fails to control the propagation of the growing polymeric chain.[49] Note that the SC-ATRP in absence of deactivator ($CuCl_2$) leads to poor (20.5%) grafting of polymer. The grafting is also low (8.3%) when CuCl/bpy is used as catalyst along with 10 wt% Cu (II) (Figure S6A and Table S1 in the Supporting Information). Also, MWDs of the obtained polymers were broader in these two cases (Figure S6B and Table S1 in the Supporting Information). FTIR spectrum (Figure S1A in the Supporting Information) of the obtained MSPN hybrids showed bands corresponding to both carbonyl vibration of poly(methacrylate)s at 1730 cm^{-1} and Si-O-Si linkage of silica at 1068 cm^{-1}.[47] TGA thermograms of MSPN hybrids (Figure S3 in the Supporting Information) show a significant weight losses (temperature range from 120 °C to 800 °C), which are attributable to the initiator and poly(methacrylate) assuming their complete decomposition, as the silica remains thermally stable at that temperature range. The obtained MS[poly(methyl methacrylate)] nanospheres (MSPMMAN), MS[poly(benzyl methacrylate)] nanospheres (MSPBzMAN), MS[poly(n-butyl methacrylate)] nanospheres (MSPnBMAN) and MS[poly(t-butyl methacrylate)] nanospheres (MSPtBMAN), hybrids obtained after 48 h of polymerization contained 67.9, 63, 53 and 52% of the corresponding poly(methacrylate)s, respectively (Figure S3 in the Supporting Information). The S_{BET} of MSPMMAN was

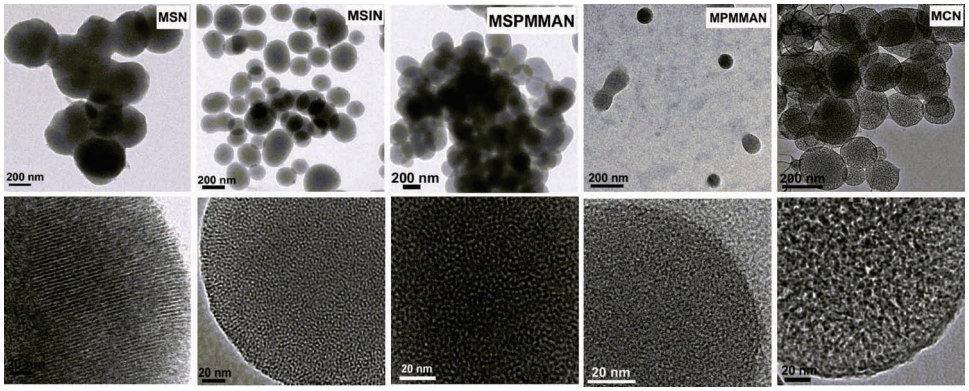

Figure 3. TEM images of different mesoporous nanospheres (upper panels). The high-magnification TEM images of the corresponding nanospheres (lower panels).

reduced to 90 m^2 g^{-1} from 1200 m^2 g^{-1}, while the total pore volume also decreased from 0.703 to 0.048 cc g^{-1} (Figure S2 in the Supporting Information and Table 1). Similar results were obtained for MSPBzMAN hybrids (Figure S7 and Table S2 in the Supporting Information). These data confirms that the pores are grafted with polymers. XRD pattern of a representative MSPMMAN hybrid (Figure 1A) reveals a diffraction peak at $2\theta = 2.75°$, which suggests that the mesoporous network of the silica template remains intact even after polymer incorporation into the porous channel. The reduction in the intensity of the diffraction peak compared to that of MSIN is due to pore filling by the polymer.[50] The XRD patterns of other MSPN hybrids (MSPBzMAN, MSPnBMAN and MSPtBMAN) also show similar results (Figure S8A in the Supporting Information). DSC thermogram of the MSPMMAN hybrid exhibited a flat trace indicating absence of glass transition temperature (T_g). But, the MPMMAN (after etching silica template with HF as discussed later) showed a clear T_g at around 105 °C (Figure S9 in the Supporting Information). The absence of T_g in the MSPMMAN hybrid is due to restriction imposed on the collective motion of the PMMA chains confined to low dimensionality spaces.[37] As expected, FESEM image clearly shows that the external spherical shape of the MSIN template remains unchanged after PMMA grafting into its mesopores (Figure 2). The size of the MSPMMAN (172–340 nm) is also comparable to the size of MSIN template (166–381 nm) (Table 1). The TEM image (Figure 3) also shows the spherical MSPMMAN hybrid. High magnification TEM image of this hybrid show that the original mesostructure of MSIN is almost retained even after grafting with PMMA. FESEM-EDX analysis reveals increase in carbon content in MSPMMAN sample (C:O:Si = 29.5:60.7:9.8) compared to MSIN sample (C:O:Si = 2.4:53.1:44.5) confirming grafting of polymer (Figure S4). The MSPMMAN samples' suspension was analyzed via DLS. The lognormal distribution of the size of the MSPMMAN in ethanol reveals a D_h value of 262 nm (Figure S5B and Table 1). This D_h value is correlated well with the diameter of the MSPMMAN measured by FESEM and TEM (Table 1).

In order to study the kinetics of the MMA polymerization initiated from the pore surface of MSIN, known aliquot mixtures were taken out at different time intervals and the amount of grafted polymer was measured from the TGA analysis of MSPMMAN hybrids obtained at different time (Figure S10A in the Supporting Information). **Figure 4**A revealed steady increase of percentage grafting of PMMA into the mesoporous channel of MSIN from 51.9 to 71.4% with polymerization time. The percentage grafting attained after 48 h of polymerization is likely to correspond to a nearly complete filling of the mesopores of MSIN.

2.3. Mesoporous Polymer Nanospheres (MPN)

In general, the MPN were prepared from the aqueous suspension of MSPN hybrid (polymerization time = 48 h) through dissolution of silica framework with aqueous HF solution. The obtained MPN are soluble in various organic solvents because the polymer chains are no longer grafted to silica framework, indicating the complete etching of silica. FTIR spectrum of the representative mesoporous poly(methyl metacrylate) nanospheres (MPMMAN) showed carbonyl band (at ~1730 cm^{-1}) for PMMA and are similar to the spectrum of the neat PMMA (Figure S1B in the Supporting Information). Notably, no band of Si-O-Si bond of silica was observed. From FESEM image (Figure 2), it can be clearly seen that the MPMMAN inherited their parents' spherical morphology with diameter in the range of 156–299 nm, which is almost same to that (172–340 nm) of MSPMMAN hybrid. The size of the MPMMAN shifts to smaller value (89–146 nm) under TEM observation (Figure 3) compared to that obtained from FESEM (see Table 1). Note that this reduction of size of MPMMAN is probably due to its shrinkage, when observed under an accelerating voltage of 100 kV. The disordered arrangement of the mesopores in MPMMAN is due to the presence of a non-interconnecting one dimensional channel network in the host MCM-41 type MSIN.[51] FESEM-EDX analysis (Figure S4, Supporting Information) reveals the presence of C and O in the atom% ratio of C:O = 79.1:20.9. DLS analysis reveals that the D_h of the MPMMAN in ethanol is 191 nm (Figure S5B in the Supporting Information and Table 1), which is in good correlation with the diameter of the

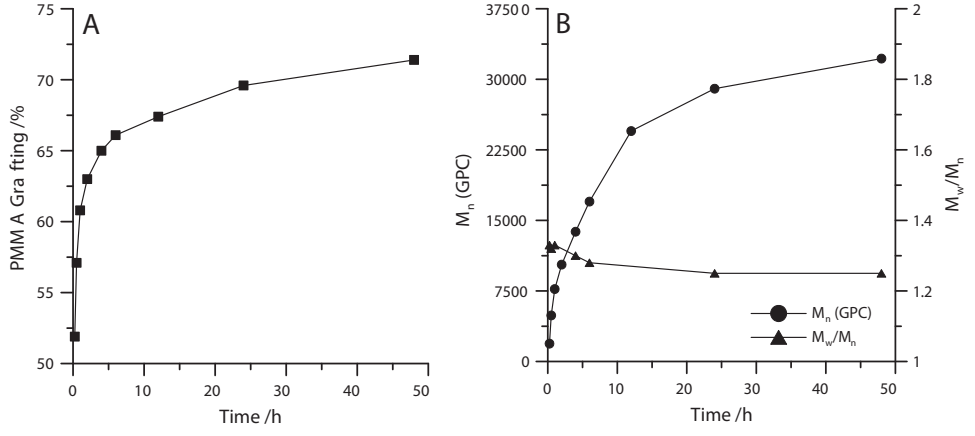

Figure 4. A) Plot of % PMMA grafting into the mesopores of MSIN vs time. B) Dependence of M_n and PDIs of the cleaved MPMMAN with polymerization time. Conditions: $[M]_0/[I]_0/[CuCl]_0/[CuCl_2]_0/[PMDETA]_0 = 200:1:1:0.1:1.1$.

nanospheres measured by FESEM and TEM (see Table 1). The retention of size, spherical morphology and porosity may be explained as follows: Due to the high polymer grafting (>60%) in the MSPMMAN hybrid, polymer bundles formed in the mesoporous channel of the MSIN template are rigid enough to hold the structure even after removal of silica template. N_2-sorption analysis further confirms the mesostructures of the MPMMAN replica (Figure S2 in the Supporting Information) with S_{BET} of 520 m^2 g^{-1}, the total pore volume of 0.190 cc g^{-1} and an average pore diameter of 1.62 nm (Table 1). Similarly, the S_{BET}, pore volume and average pore diameter of MPBzMAN were found to be 382 m^2 g^{-1}, 0.177 cc g^{-1} and 1.93 nm, respectively (Figure S7 and Table S2 in the Supporting Information). XRD pattern of the MPMMAN exhibit a peak at around 2θ = 2.75°, which further confirms the presence of ordered mesopores (Figure 1A). Similar results were obtained with other MPN (MPBzMAN, MPnBMAN and MPtBMAN) (Figure S8B in the Supporting Information). The intensity of this diffraction peak is low and broad compared to that of MSIN. This is probably due to the absence of a rigid silica pore structure and shrinkage of the pores in the MPN. TGA thermograms of representative MPMMAN and MPBzMAN samples (Figure S11 in the Supporting Information) revealed a rapid weight loss at around 230 °C indicating that these nanospheres are made up of only polymer.

Cross-linked MSPMMAN hybrid were prepared using 15 mol% EGDMA (with respect to MMA) as the cross-linker using a polymerization time of 48 h. The obtained cross-linked MPMMAN after removal of silica framework, however, are not soluble in common organic solvents. FESEM image of such cross-linked MPMMAN is shown in Figure S12 in the Supporting Information, which reveals that the spherical shape of the template MSIN (Figure 2) is retained in the cross-linked MPMMAN.

The molecular weights of cleaved MPN were measured by GPC after dissolving in THF. The MPMMAN obtained at different polymerization time showed narrow unimodal MWDs (Figure S10B in the Supporting Information) and a very clear gradual lateral shift towards high molecular weight region with time. The M_n (GPC) of the cleaved PMMA increased almost linearly at the initial period of polymerization, but after a polymerization time of 12 h, the curve deviated from linearity. The PDI remained narrow (~1.3) and decreased slowly with polymerization time (Figure 4B), as normally expected from a controlled radical polymerization.[52] GPC traces of the other MPN samples also displayed a narrow unimodal MWD with a PDI of <1.3 (**Table 2** and Figure S13 in the Supporting Information) suggesting that this SC-ATRP proceed in a well-controlled manner.

Table 2. Molecular characterization data for different cleaved poly(methacrylate)s obtained by SC-ATRP using MSIN as the template.

Sample	$M_{n,theo.}$ [kDa]	$M_{n,GPC}$ [kDa]	PDI [M_w/M_n]
MPMMAN	20.0	31.1	1.25
MPBzMAN	35.2	33.0	1.28
MPnBMAN	28.4	41.0	1.30
MPtBMAN	28.4	51.6	1.29

Conditions: $[M]_0/[I]_0/[CuCl]_0/[CuCl_2]_0/[PMDETA]_0$ = 200:1:1:0.1:1.1. Solvent = xylene; Temperature = 105 °C; Time = 48 h.

2.4. MP Nanospheres as Low Dielectric Constant (Low-*k*) Materials

Figure 5 shows the dielectric constants (k) of MSIN, MSPMMAN hybrid and MPMMAN samples over a frequency range from 10 kHz to 10 MHz. Notably, the dielectric constant of the MPMMAN (k = 9.31) is the lowest among the three. Dielectric losses (ε'') are low and negative in certain frequency regions in the cases of MSPMMAN hybrid and MPMMAN (see Figure S14 in the Supporting Information). The combination of advantages such as high thermal stabilities, low-k, low dielectric loss, ordered mesostructure, and controllable morphology for mesoporous materials, especially MPN materials, described above makes them a potential candidate for use as heat insulators and dielectric and packaging materials in microelectronic products.[53]

2.5. Functional MSPN Hybrid/MPN and their Applications

2.5.1. MS[Poly(methyl methacrylate)-co-poly(4-vinyl benzyl chloride)] Nanospheres [MS(PMMA-co-PVBC)N]hybrid/ M[poly(methyl methacrylate-co-poly(4-vinyl benzyl chloride)] Nanospheres[M(PMMA-co-PVBC)N]

Benzyl chloride functionalized hybrid nanospheres were prepared using VBC (20 mol%) as comonomer with MMA

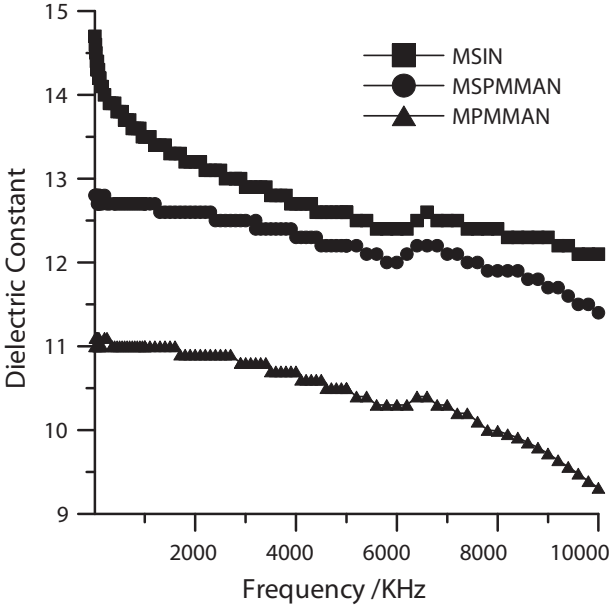

Figure 5. Dielectric constants of different mesoporous nanospheres as a function of frequency.

(**Scheme 2**). FTIR spectrum of the MS(PMMA-co-PVBC)N hybrid (Figure S15A in the Supporting Information) reveal the band of Si-O-Si linkage at around 1082 cm^{-1} and carbonyl band of PMMA at 1732 cm^{-1}. Additional bands were also observed at 1452, 1510 and 1633 cm^{-1} due to phenyl ring stretching vibration; 1437 cm^{-1} due to CH_2 of chloromethyl group; 750 cm^{-1} due to C-Cl stretching vibration and 664 cm^{-1} due to typical benzene-ring stretching. All these bands confirm the presence of both PMMA and PVBC unit in the MS(PMMA-co-PVBC)N hybrid. TGA thermogram of the hybrid (Figure S16 in the Supporting Information) revealed 57.9% grafting of the functional polymer into the MSIN. XRD pattern of the M(PMMA-co-PVBC)N, obtained after removal of silica template (Figure S17 in the Supporting Information) showed a diffraction peak at $2\theta = 2.75°$, characteristic of mesostructures. FESEM images clearly showed that both the MS(PMMA-co-PVBC)N hybrid and the M(PMMA-co-PVBC)N are spherical in shape (Figure S18 in the Supporting Information), indicating the spherical shape of the MSIN is remained. GPC trace (Figure S19 in the Supporting Information) of the M(PMMA-co-PVBC)N reveals a narrow unimodal MWD with PDI = 1.29 and molecular weight of 31100.

Next, we explored chemical post-functionalization of the M(PMMA-*co*-PVBC)N by using -CH_2Cl group that originated from 4-vinylbenzyl chloride (VBC) monomer. The–CH_2Cl group allows "click" process to introduce–CH_2N_3 group by reaction with NaN_3 (Scheme 2, see the Supporting Information for synthesis protocol). FTIR spectrum (Figure S20 in the Supporting Information) reveals a band at 2104 cm^{-1} confirming the presence of azide group in the M(PMMA-*co*-PVBC)N. Copper-catalyzed azide–alkyne cycloaddition reaction was then used to prepare triazole functionalized M(PMMA-*co*-PVBC)N by the reaction of this azide group with phenyl acetylene as model compound (Scheme 2, see the Supporting Information for detailed procedure).[54] FTIR spectrum reveals a band in the region of 1650–1570 cm^{-1} due to ring stretching vibrations of triazole ring (Figure S20 in the Supporting Information).[55] This approach developed by us will open up an area to synthesize MPN functionalized with triazole moiety having antimicrobial activity.[56]

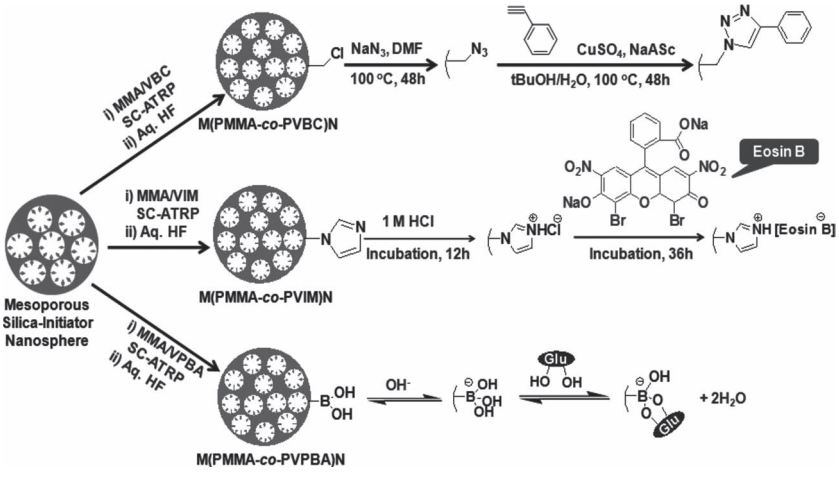

Scheme 2. Schematic illustrations of A) synthesis of triazole functionalized MPMMAN (MP-CH_2-Htrz) by click chemistry; B) anionic dye exchange by protonated M(PMMA-*co*-PVIM)N, and C) glucose sensing by M(PMMA-*co*-PVPBA)N.

2.5.2. MS[Poly(methyl methacrylate)-co-poly(vinyl imidazole] Nanospheres [MS(PMMA-co-PVIM)N] Hybrid/M[Poly(methyl methacrylate-co-poly(vinyl imidazole)] Nanospheres [M(PMMA-co-PVIM)N]

Imidazole functionalized MS(PMMA-*co*-PVIM)N hybrid and M(PMMA-*co*-PVIM)N were also prepared by similar procedure (Scheme 2). FTIR spectrum of the hybrid (Figure S15A in the Supporting Information) shows bands for imidazole ring (1650–1570 cm^{-1})[55] along with the bands of Si-O-Si linkage (1086 cm^{-1}) and carbonyl stretching (1732 cm^{-1}) of PMMA. TGA thermogram of this hybrid (Figure S16 in the Supporting Information) revealed 38.2% grafting of this functional copolymer into the mesopore of MSIN. XRD pattern of M(PMMA-*co*-PVIM)N (Figure S17 in the Supporting Information) showed a diffraction peak at $2\theta = 2.75°$ (as discussed above) suggesting the presence of mesoporous network. FESEM image reveals that the spherical shape of the MSIN template is retained both in the hybrid and M(PMMA-*co*-PVIM)N (Figure S18 in the Supporting Information). M_n and M_w/M_n of the M(PMMA-*co*-PVIM)N were found to be 33 000 and 1.26 respectively as analyzed from the GPC chromatograph (Figure S19 in the Supporting Information).

The anion exchange ability of the as-synthesized protonated M(PMMA-*co*-PVIM)N ($[MP\text{-}NH]^+[Cl]^-$) (see the Supporting Information for the protonation protocol) was studied using a monoanionic dye, Eosin B and the exchange capacity was monitored by UV-vis spectroscopy. A gradual decrease of absorbance of Eosin B at 517 nm with time was observed (**Figure 6**A) and the calculation revealed that ~82% dye was exchanged after incubation for 36 h (inset of Figure 6A). This corresponds to binding of 0.345 mmol of Eosin B per gram of $[MP\text{-}NH]^+[Cl]^-$. The fluorescence emission spectrum of $[MP\text{-}NH]^+[Eosin\ B]^-$ conjugate showed a clear shift of the emission maximum from 549 nm (for pure Eosin B) to 590 nm (Figure 6B). This shift (41 nm) confirms successful exchange of Cl^- of $[MP\text{-}NH^+][Cl]^-$ with Eosin B. Fluorescence light microscopic image (Figure 6C) further conforms successful exchange of Eosin B, producing red light emitting beads of $[MP\text{-}NH]^+[Eosin\ B]^-$ conjugate. Fluorescence lifetime experiment was performed to study the exchange of Eosin B with $[MP\text{-}NH]^+[Cl]^-$ (Figure S21 in the Supporting Information) and the data (fluorescence decay traces) were fitted with the equation given below,

$$I(t) = \sum_{i=1}^{N} A_i \exp\left(\frac{-t}{\tau_i}\right)$$

where, A_i is the relative amplitude of the *i*-th fluorescence component, τ_i is the lifetime of the *i*-th fluorescence component and N is the number of the fluorescence exponentials required for best Nonlinear Least Square (NLLS) fitting of the fluorescence decay curves. There is a significant difference in the fluorescence decay behavior of Eosin B in solution state and in bound state as $[MP\text{-}NH]^+[Eosin\ B]^-$ conjugate (**Table 3**). This difference might be due to the fact that the excited state of bound-Eosin B become less stabilized compared to that of unbound form in water

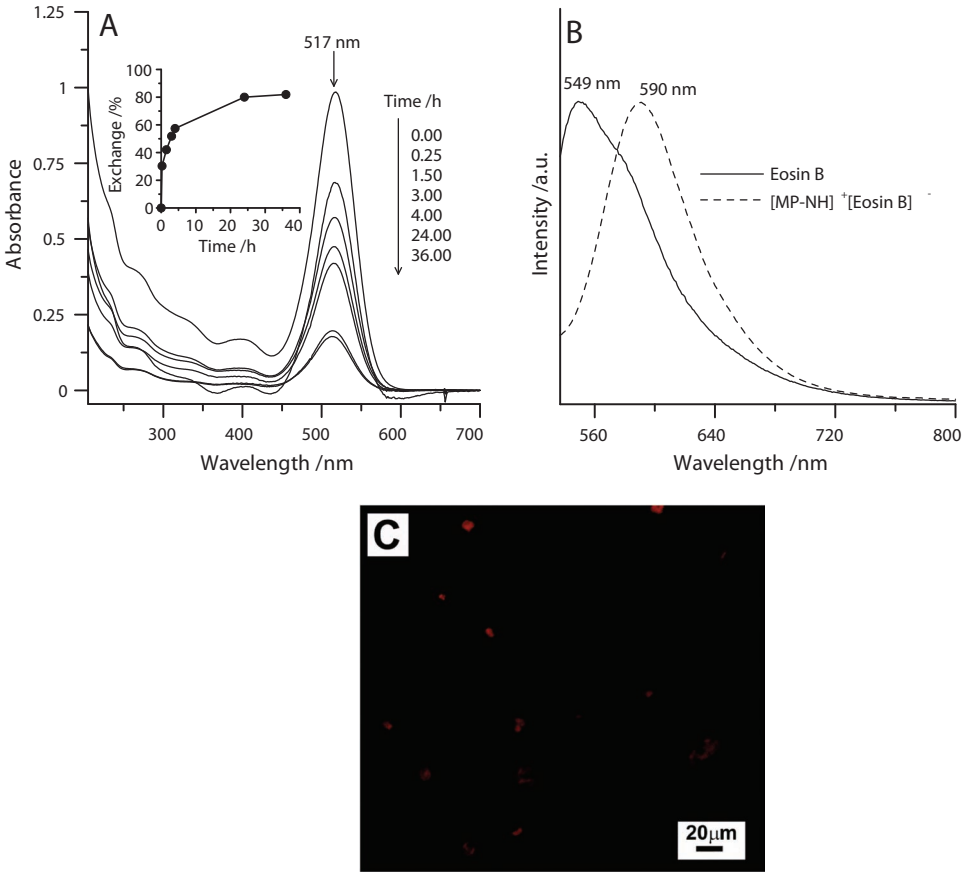

Figure 6. A) Successive UV-vis absorption spectra of Eosin B after incubating with $[MP\text{-}NH]]^{+}[Cl]^{-}$ for different times. The inset shows the plot of% exchange of Eosin B vs time. B) Fluorescence emission spectra of aqueous solution of Eosin B and aqueous suspension of $[MP\text{-}NH]^{+}[Eosin\ B]^{-}$ conjugate. C) Fluorescent light microscopy images of $[MP\text{-}NH]^{+}[Eosin\ B]^{-}$ conjugates.

and simultaneous relaxation from the multiple excited electronic states occur.[57] This successful anion exchange capability of $[MP\text{-}NH]^{+}[Cl]^{-}$ nanospheres opens up new possibilities for removal of anionic organic pollutants from contaminated water.

2.5.3. MS[Poly(methyl methacrylate)-co-poly(4-vinylphenylboronic acid)] Nanospheres [MS(PMMA-co-PVPBA)N]hybrid/ M[poly(methyl methacrylate-co-(4-vinylphenylboronic acid)] Nanospheres [M(PMMA-co-PVPBA)N]

Boronic acid functionalized MS(PMMA-*co*-PVPBA)N hybrid and M(PMMA-*co*-PVPBA)N were prepared by similar procedure using VPBA as comonomer as mentioned above (Scheme 2). FTIR spectra of the MS(PMMA-*co*-PVPBA)N hybrid (Figure S15A in the Supporting Information) shows bands for phenyl ring stretching vibration (1635 cm^{-1}), H-bonded OH of–$B(OH)_2$ moiety (~3441 cm^{-1}),[58] Si-O-Si linkage of silica (1086 cm^{-1}) and carbonyl stretching of PMMA (1730 cm^{-1}). TGA thermogram of the hybrid (Figure S16 in the Supporting Information) revealed the presence of 23.4% functional polymer in the hybrid. The presence of a diffraction peak at $2\theta = 2.75°$ in the XRD pattern of the M(PMMA-*co*-PVPBA)N (Figure S17 in the Supporting Information) suggests that the mesoporous structure is maintained in this functional nanospheres. FESEM image of the functional MS(PMMA-*co*-PVPBA)N hybrid and pure M(PMMA-*co*-PVPBA)N (Figure S18 in the Supporting

Table 3. Nonlinear least square (NLLS) fitting parameters obtained from the fluorescence decay curves using the given equation.

Sample	A_1	τ_1 [ns]	A_2	τ_2 [ns]	A_3	τ_3 [ns]	A_4	τ_4 [ns]	χ^2
Eosin B	0.52	1.06	0.09	3.26	0.039	0.03	–	–	2.92
$[MP\text{-}NH]^{+}[Eosin\ B]^{-}$	0.28	0.21	0.16	0.86	0.1	2.62	0.46	0.02	1.39
FITC-ConA	0.30	1.51	0.09	0.03	0.61	3.69	–	–	1.51
MP-Glu-ConA-FITC	0.99	0.008	0.01	1.83	–	–	–	–	0.29

Excitation wavelength: 440 nm. Detection wavelength: 549 nm for Eosin B, 590 nm for $[MP\text{-}NH]^{+}[Eosin\ B]^{-}$ and 520 nm for FITC-ConA and MP-Glu-ConA-FITC.

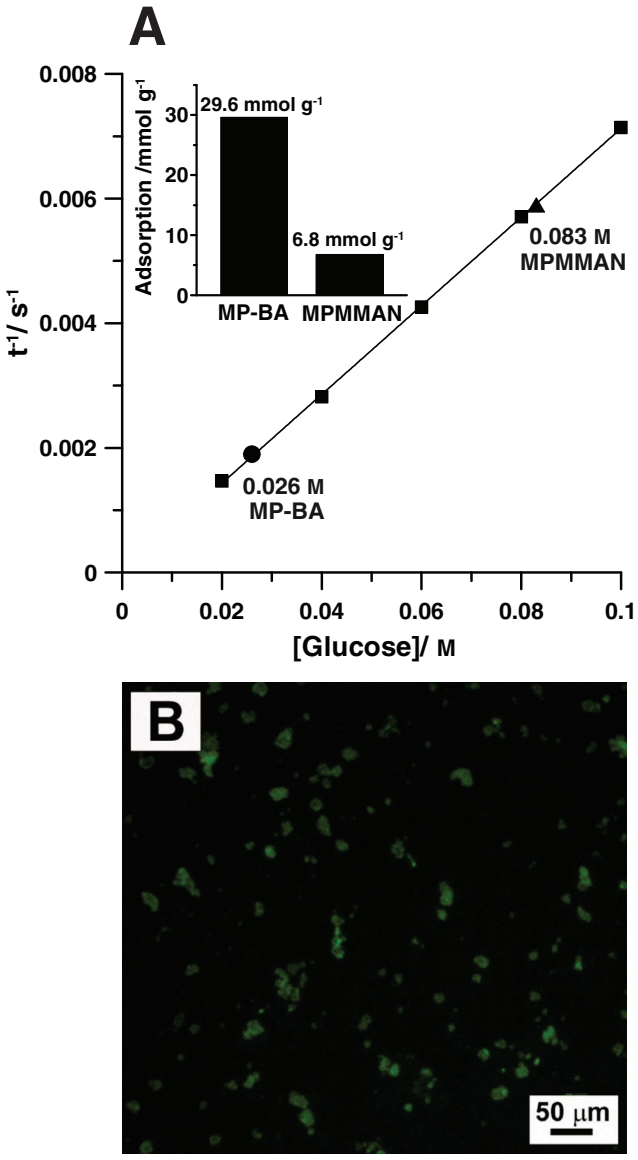

Figure 7. A) Plot of t^{-1} vs glucose concentration obtained from the colorimetric estimation of glucose concentration in solution. Inset shows plot of amount of glucose adsorbed by different MPN. B) Fluorescent light microscopy image of MP-Glu-ConA-FITC nanospheres.

Information) clearly reveal the retention of the spherical shape of the initial silica (MSIN) template. GPC (Figure S19 in the Supporting Information) analysis of M(PMMA-*co*-PVPBA)N reveals a narrow unimodal MWD with M_n and M_w/M_n values of 21 200 and 1.32 respectively.

Glucose sensing ability of the M(PMMA-*co*-PVPBA)N (MP-BA) was studied by incubating the nanospheres in the solution of dextrose in phosphate buffered saline (PBS) (0.1 M, pH 7.4) for 24 h (see the Supporting Information for detailed procedure). As a control experiment, MPMMAN was similarly incubated with the same dextrose solution. After complete incubation, the remaining glucose concentration in the solution was determined by the colorimetric estimation method (see the Supporting Information for detailed procedure). **Figure 7**A revealed that starting with a 0.1 M glucose concentration, final glucose concentration was found to be 0.026 M and 0.083 M in case of M(PMMA-*co*-PVPBA)N and MPMMAN respectively. This gives an estimate of binding of 29.6 and 6.8 mmol of glucose per gram of M(PMMA-*co*-PVPBA)N and MPMMAN, respectively. Hence, it can be concluded that M(PMMA-*co*-PVPBA)N is more effective in glucose binding than MPMMAN. To further confirm successful glucose binding, we prepare FITC-ConA conjugate using a reported protocol,[59] where ConA is a carbohydrate-binding protein and FITC is a fluorescent marker. FITC-ConA was then incubated with dextrose bound (MP-Glu) nanospheres. Fluorescence light microscopic image (Figure 7B) clearly shows that the FITC-ConA indeed binds with MP-Glu nanospheres, producing green light emitting beads. Fluorescence lifetime experiment was performed to study the binding of FITC-ConA with MP-Glu nanospheres (Figure S22 in the Supporting Information) and the data are summarized in Table 3. The decrease of fluorescence lifetime for MP-Glu-ConA-FITC is possibly due to quenching of fluorescence of FITC-ConA when bound to MP-Glu nanospheres leading to very fast deactivation.

2.6. Mesoporous Carbon Nanospheres (MCN)

MCN was synthesized from the MSPMMAN hybrid by carbonization and subsequent dissolution of silica framework by HF. As expected, the FTIR spectrum of both the mesoporous silica-carbon hybrid nanospheres (MSCN) and the as-synthesized MCN (Figure S23 in the Supporting Information) exhibits carbonyl stretching band at ~1732 cm^{-1}, C = C stretching band at ~1630 cm^{-1}, CH_2 asymmetric band at ~2922 cm^{-1} and CH_2 symmetric band at ~2852 cm^{-1}, which is probably due to the adsorbed gaseous MMA monomer formed during the pyrolysis of grafted PMMA at above 450 °C as suggested by other researchers.[60] Further, the spectrum of MCN (Figure S23b in the Supporting Information), did not show any band of Si-O-Si linkage of silica, and also the CH_2 asymmetric and CH_2 symmetric bands are more intense than MSCN, indicating complete etching of silica framework. FESEM images of MSCN hybrid (Figure S24 in the Supporting Information) and MCN (Figure 2) reveal that both of them retain the spherical shape of the initial MSIN with diameters very close to that of MSIN (Table 1). The high magnification TEM image of the MCN (Figure 3) displayed well developed, roughly spherical, and quite closely packed mesopores throughout the entire MCN. FESEM-EDX spectrum of the MCN (Figure S4 in the Supporting Information) exhibits only an intense peak due to elemental carbon with a low intense peak due to elemental oxygen. The lognormal distributions of the size of MCN obtained from its ethanol suspension reveals that the D_h of the MCN is about 1620 nm (Figure S5B and Table 1). Note that the D_h value is higher than the diameter obtained from FESEM and TEM. This is probably due to some aggregation of the carbon nanospheres in ethanol. The S_{BET} of the MCN was found to be 658 $m^2\ g^{-1}$ with average pore size around 5.66 nm and the total pore volume of 0.54 cc g^{-1} (Table 1), as determined from the N_2 adsorption isotherm of MCN (Figure S2 in the Supporting Information). MCN with such higher pore diameters are highly desirable for practical

use.[9,11,12] The XRD pattern of the MCN (Figure 1B) showed a strong peak centered at ~24° and a less intense peak at ~44° and a hardly detectable broad feature at ~80°. These peaks can be ascribed to (002), (101) and (110) peaks of a graphitic carbon structure.[27] The aqueous suspension of MCN exhibits blue fluorescence when irradiated with UV light (inset of Figure S25A in the Supporting Information). The MCN suspension gives a scattered UV-vis absorption spectral peak (Figure S25A in the Supporting Information). Fluorescence emission spectra of the aqueous suspension of MCN were taken at different excitations (Figure S25B in the Supporting Information). These spectra reveal an emission maximum at 410 nm with the highest fluorescence intensity when excited at a wavelength of 300 nm.

3. Conclusions

The successful surface-confined ATRP process from initiator-modified mesoporous silica nanospheres template followed by silica removal by etching produced mesoporous polymer and mesoporous carbon nanospheres with complete retention of the shape of the original template, as confirmed via FESEM and TEM. The absence of silica framework in mesoporous polymer and mesoporous carbon materials was confirmed using FTIR spectroscopy. The "living" nature of this polymerization was confirmed from a kinetic study of the methacrylate polymerization and successful synthesis of poly(methacrylates)s with controlled molecular weights and narrow polydispersities (PDI < 1.3). The as-synthesized mesoporous polymer showed low dielectric constants and therefore they can be used as a promising material in microelectronics. This approach allowed the fabrication of functional mesoporous polymer nanospheres. These functional mesoporous polymer were successfully used for the synthesis of "clickable" mesoporous polymer, removal of anionic contaminates through ion exchange, and glucose sensing. Finally, this approach may allow for the fabrication of different shapes of porous polymeric/carbon materials produced from a variety of templates. Additionally, the functional mesoporous polymer/carbon materials with different shapes are the highly promising multifunctional materials for diverse applications.

4. Experimental Section

Materials: Tetraethyl orthosilicate (TEOS), copper (I) chloride (CuCl), copper (II) chloride ($CuCl_2$), 2,2′-bipyridyl (bpy), *N,N,N′,N″,N″*-pentamethyldiethylenetriamine (PMDETA), activated basic aluminium oxide (Al_2O_3), 4-vinylphenylboronic acid (VPBA), L-ascorbic acid, phenylacetylene, Eosin B, fluorescein isothiocyanate (FITC) and concanavalin A (ConA) were purchased from Aldrich and were used as received. Cetyltrimethylammonium bromide (CTAB, Loba Chemie, India) and ((chloromethyl)phenylethyl)trimethoxysilane (CMPE-TMS, Gelest Inc.) were used as received. Methyl methacrylate (MMA) (Burgoyne Urbridges and Co.) was washed with 5 wt% aqueous NaOH solution to remove the inhibitor, dried overnight with calcium chloride ($CaCl_2$) and then distilled over calcium hydride (CaH_2) under reduced pressure prior to use. The other monomers such as benzyl methacrylate (BzMA), n-butyl methacrylate (nBMA), t-butyl methacrylate (tBMA), ethylene glycol dimethacrylate (EGDMA), 4-vinylbenzyl chloride (VBC) and 1-vinylimidazole (VIM) were obtained from Aldrich and were purified by passing through a column filled with basic aluminum oxide to remove inhibitor prior to use. Copper (II) sulfate pentahydrate ($CuSO_4.5H_2O$), sodium azide (NaN_3), 40% hydrofluoric acid (GR), dextrose anhydrous, sodium hydroxide, tetrahydrofuran (THF) and methanol were obtained from Merck, India and used as received. Xylene (Merck, India) was dried and purified by refluxing over sodium/benzophenone just before use. Tert-butyl alcohol (tBuOH, Merck, India) was distilled over calcium hydride just before use. DMF was distilled over calcium hydride under reduced pressure just before use. Triple distilled water was used for making all the aqueous solutions/suspensions.

Synthesis of Mesoporous Silica Initiator Nanospheres (MSIN): The procedure described here is based on the modification of the method reported earlier by Lin et al.[45] The in situ immobilization of ATRP initiator was carried out by co-condensation of TEOS and CMPE-TMS (contains three trimethoxysilyl group and (chloromethyl)phenylethyl (CMPE) ATRP initiator moiety) (Scheme 1). In a typical synthesis, a mixture of CTAB (1.6 g, 4.4 mmol), aqueous NaOH (5.6 mL of 2.0 M, 11.2 mmol), and H_2O (385 mL, 21.3 mol) were taken in a round bottomed flask (500 mL). The mixture was heated at 80 °C for 30 min with continuous magnetic stirring to get a clear solution. The pH of the reaction mixture was around 12. TEOS (7.95 mL, 35.9 mmol) and CMPE-TMS (1.15 mL, 4.6 mmol) were added sequentially and rapidly to this clear solution. A white precipitation was observed soon after the addition of TEOS and CMPE-TMS. The reaction mixture was further stirred for another 2 h at that temperature. The product was isolated by hot filtration. It was then washed repeatedly with water and methanol and dried under vacuum. The CTAB (template) was removed by the following procedure. A methanolic HCl solution (200 mL of methanol and 2.0 mL of concentrated HCl) was added to of as-synthesized material (2.0 g) and was heated at 60 °C for 6 h with stirring. The resultant MSIN was isolated by filtration and washed repeatedly with water and methanol and dried under vacuum at 80 °C and kept in desiccators for further use as macroinitiators to initiate the ATRP processes. A neat mesoporous silica nanosphere (MSN) was also prepared using similar procedure described above in the absence of CMPE-TMS.

Preparation of MSPNs by SC-ATRP of Methacrylate Monomers: In a typical experiment, the molar ratio of the reactants is as follows: monomer:I:CuCl:$CuCl_2$:PMDETA = 200:1:1:0.1:1.1. The synthesis procedure is schematically given in Scheme 1. For mesoporous silica-poly(methyl methacrylate) hybrid (MSPMMAN) preparation, typically, MSIN (0.216 g, 0.115 mmol) was taken in a long neck round bottom flask (25 mL) and was heated at 100 °C for 4 h under vacuum to remove any trapped moisture or any other gaseous entity and temporarily sealed with a silicone rubber septum. Dry xylene (2.5 mL), previously purged with dry nitrogen for 15 min, was then added to the flask using a dry syringe and was further purged with nitrogen for 15 min to remove any residual oxygen from the system. CuCl (11.4 mg, 0.115 mmol), $CuCl_2$ (1.5 mg, 0.0115 mmol) and PMDETA (26 µL, 0.126 mmol) were then added to the mixture and was again purged with nitrogen for another 30 min. Freshly distilled and nitrogen purged MMA (2.5 mL, 23.0 mmol) was then injected by a syringe. The reaction mixture was again purged with nitrogen for another 20 min under magnetic stirring to ensure the removal of any trace of oxygen from the system. The flask was then permanently sealed with silicone rubber septum. The reaction mixture was then sonicated for 1 min to increase dispersity in xylene and placed in a silicone oil bath thermostated at 105 °C with constant magnetic stirring. After the specified reaction time, the polymerization was stopped via exposure to air. For kinetics study, polymerization was carried out in nine different flasks and stopped at different time intervals from 15 min to 48 h. A similar procedure was adopted for SC-ATRP of other methacrylate monomers such as BzMA, nBMA and tBMA from MSIN. After polymerization, the MSPN hybrids were isolated by centrifugation at 10 000 rpm for 30 min and then thoroughly washed with THF and methanol successively by three repeated cycles of dispersion-centrifugation. The isolated hybrids were dried at 80 °C for 24 h under vacuum. Finally, functional MSPMMAN hybrids such as MS(PMMA-*co*-PVBC)N, MS(PMMA-*co*-PVIM)N and MS(PMMA-*co*-PVPBA)N were prepared by adding 20 mol% of functional monomers such as VBC or VIM or VPBA with respect to MMA, keeping all other reaction parameters constant (Scheme 2).

Preparation of MPNs: Typically, the obtained MSPMMAN hybrid was first suspended in water in a plastic container. An aqueous HF solution (10 wt%) was then added to suspension and was kept undisturbed for 12 h for complete etching of silica template (Scheme 1). Caution: HF is extremely corrosive. The resulting template free mesoporous PMMA (MPMMAN) was obtained as an insoluble component. It was collected by centrifugation (10000 rpm for 30 min) and thoroughly washed with water by repeated cycles of dispersion-centrifugation (10 000 rpm for 30 min) to remove excess HF until neutral pH was achieved. Finally, the MPMMAN was dried under vacuum at 80 °C for 24 h.

Preparation of MCNs: At first, the purified MSPMMAN hybrid was converted to mesoporous silica-carbon (MSCN) hybrid by the following procedure (Scheme 1). MSPMMAN was first heated under air at 250 °C to stabilize the PMMA. At this temperature (250 °C), the air was switched to nitrogen and purging was continued for an hour and then the heating was continued to reach 800 °C, and the latter temperature was maintained for 6 h to pyrolize the polymer and finally cooled to room temperature.[27] The obtained MSCN hybrid was then suspended in water in a plastic container and a 10 wt% aqueous HF solution was added and kept for 12 h to etch out silica completely. Silica free mesoporous carbon (MCN) was collected by centrifugation (10 000 rpm for 30 min) and thoroughly washed with water by repeated cycles of dispersion-centrifugation (10 000 rpm for 30 min) to remove excess HF until neutral pH was achieved. Finally, MCN was dried at 80 °C for 24 h under vacuum.

Characterization: The X-ray diffraction (XRD) measurement of the dried mesoporous materials were carried on a Bruker AXS D8 diffractometer at an acceleration voltage of 40 kV with 40 mA current intensity using Cu tube ($\lambda = 0.154$ nm) as radiation source.

FTIR spectra of all the samples (except MPN) were recorded from KBr pellets, prepared by mixing respective dried samples with dried KBr {in 1:100 (wt/wt) ratio} in a Perkin Elmer FTIR Spectrum-400 spectrometer. The spectrum of the etched MPN was obtained by casting one drop of a THF solution on KBr pellet.

The purified and dried mesoporous samples were subjected to thermogravimetric analysis under air using a TA SDT Q 600 instrument at a heating rate of 20 °C min^{-1} from room temperature to 800 °C.

Nitrogen sorption measurements were performed using a Quantachrome Autosorb-1 at 77 K. The Brunauer–Emmett–Teller (BET) surface area was deduced from the isotherm analysis. The pore size distribution (PSD) was calculated by means of the Barrett–Joyner–Halenda (BJH) method.

The glass transition temperature (T_g) of MSPMMAN and MPMMAN materials were measured using a differential scanning calorimeter (Q2000, TA Instruments) under N_2 atmosphere. The heating or cooling range was from 20 °C to 200 °C at a scanning rate of 10 °C min^{-1}, and the T_g was recorded in the second heating cycle to remove the previous thermal history of the sample.

The number average molecular weight (M_n) and polydispersity index (PDI) of the cleaved MP materials were measured by size exclusion chromatography using a Waters 1515 isocratic HPLC pump connected to three Waters Styragel HR1, HR3 and HR4 columns and a Waters 2414 refractive index detector at room temperature (25 °C). THF was used as the eluent with a flow rate of 1 mL min^{-1}. The columns were calibrated against eight narrow polystyrene standard samples with peak molecular weights (M_p) of 860, 1800, 3600, 8500, 19 100, 43 400, 50 000, and 100 000.

Field emission scanning electron microscopy (FESEM) studies were performed using a JEOL JSM-6700F electron microscope at an accelerating voltage of 5 kV. The dried mesoporous materials were dispersed in ethanol and drop casted onto a cover slip, which were then placed on a copper tape, supported on a metal stub and sputter coated with platinum to minimize charging. The elemental compositions of the mesoporous materials were measured from energy-dispersive X-ray (EDX) associated with this FESEM.

Transmission electron microscopy (TEM) studies, one drop of the ethanolic dispersion of the MSN, MSIN, MSPN, MPN and MCN were placed on a carbon-coated copper grid and allowed to dry in air. The grids were then observed on a JEOL JEM-2010 electron microscope operated at an accelerating voltage of 200 kV (except for the MPN where an accelerating voltage of 100 kV was used).

All DLS experiments were carried out at 25 °C on a Malvern Particle Size Analyzer (Model No. ZEN 3690 Zetasizer NANO ZS90). In all cases, mesoporous sample (MSN, MSIN, MSPN, MPN and MCN) (~0.01 mg) was dispersed in distilled and filtered ethanol (1 mL).

UV-vis absorption spectra of aqueous solution of Eosin B and aqueous suspension of $[MP\text{-}NH]^+[Eosin\ B]^-$ conjugate were acquired in a Hewlett-Packard 8453 UV-vis spectrophotometer.

Photoluminescence (PL) spectra of the aqueous solution of Eosin B and aqueous suspension of $[MP\text{-}NH]^+[Eosin\ B]^-$ conjugate were recorded using a Jobin-Yvon Fluoromax-3 spectrophotometer exciting the Eosin B at 517 nm.

For dielectric measurements, pellets were first prepared by pressing the dry MSIN, MSPMMAN and MPMMAN at a high pressure (7 ton) in a stainless steel die (10 mm) at room temperature. The thicknesses of the pellets were in between 1.5 and 2 mm. Finally, smoothed pellet surfaces were coated with conducting silver paste and allowed to air dry. The samples with silver electrodes were dried at 100 °C for 2 h for good contact. The dielectric response of the pellet samples were measured using Agilent Impedance Analyzer 4192A over a frequency range from 10 kHz to 10 MHz at room temperature (298 K).[61]

For time-correlated single-photon counting (TCSPC) measurements, time-resolved fluorescence spectra were acquired by TCSPC technique using a Pico second diode laser (IBH Nanoled-07) in an IBH Fluorocube apparatus. Spectra were acquired from aqueous solutions/suspensions of the samples upon excitation at 440 nm. The fluorescence decays were collected with a Hamamatsu MCP photomultiplier (C487802) and were analyzed using IBH DAS6 software.

Fluorescence microscopy images of the dye-loaded functional MPN were taken using a light microscope (BX61, Olympus) equipped with a filter set consisting of a BP530-550 nm for an exciter and a band absorbance filter covering wavelengths below 420 nm. Small quantities of the nanospheres were dispersed in water and the suspensions were placed on a glass slide and images were recorded.

Supporting Information

Supporting Information is available from the Wiley Online Library or from the author.

Acknowledgements

S.B. and T.K.P. thank CSIR, Govt. of India, for providing fellowships. The authors also thank Mr. Kaushik Chakrabarti and Prof. S. K. De, Dept. of Materials Science, IACS, for thier help to measure dielctric properties of mesoporous materials. This research was supported by the grants from the DST, New Delhi under the Nanoscience and Nanotechnology Initiative.

Received: January 27, 2012
Published online: July 3, 2012

[1] M. Hartmann, *Chem. Mater.* **2005**, *17*, 4577.
[2] F. Hoffmann, M. Cornelius, J. Morell, M. Froba, *Angew. Chem. Int. Ed.* **2006**, *45*, 3216.
[3] B. J. Scott, G. Wirnsberger, G. D. Stucky, *Chem. Mater.* **2001**, *13*, 3140.
[4] S. C. Warren, U. Wiesner, *Pure Appl. Chem.* **2009**, *81*, 73.
[5] S. Xuan, F. Wang, J. M. Y. Lai, K. W. Y. Sham, Y.-X. J. Wang, S.-F. Lee, J. C. Yu, C. H. K. Cheng, K. C.-F. Leung, *ACS Appl. Mater. Interfaces* **2011**, *3*, 237.

[6] T.-Q. Nguyen, J. Wu, V. Doan, B. J. Schwartz, S. H. Tolbert, *Science* **2000**, *288*, 652.
[7] D. L. Huber, R. P. Manginell, M. A. Samara, B.-I. Kim, B. C. Bunker, *Science* **2003**, *301*, 352.
[8] M. Choi, F. Kleitz, D. Liu, H. Y. Lee, W.-S. Ahn, R. Ryoo, *J. Am. Chem. Soc.* **2005**, *127*, 1924.
[9] S. Han, K. Sohn, T. Hyeon, *Chem. Mater.* **2000**, *12*, 3337.
[10] Y. Zhang, A. Wang, T. Zhang, *Chem. Commun.* **2010**, 862.
[11] G. S. Chai, S. B. Yoon, J.-S. Yu, J.-H. Choi, Y.-E. Sung, *J. Phys. Chem. B* **2004**, *108*, 7074.
[12] H. Zhou, S. Zhu, M. Hibino, I. Honma, M. Ichihara, *Adv. Mater.* **2003**, *15*, 2107.
[13] J. Jang, J. Bae, *Chem. Commun.* **2005**, 1200.
[14] L. M. Pitet, M. A. Amendt, M. A. Hillmyer, *J. Am. Chem. Soc.* **2010**, *132*, 8230.
[15] C. G. Goltner, M. Antonietti, *Adv. Mater.* **1997**, *9*, 431.
[16] X. Wang, C. Liang, S. Dai, *Langmuir* **2008**, *24*, 7500.
[17] U. B. Suryavanshi, T. Ijima, A. Hayashi, Y. Hayashi, M. Tanemura, *Chem. Commun.* **2011**, 10758.
[18] J. Schuster, R. Kohn, A. Keilbach, M. Doblinger, H. Amenitsch, T. Bein, *Chem. Mater.* **2009**, *21*, 5754.
[19] K. Okada, M. Nandi, J. Maruyama, T. Oka, T. Tsujimoto, K. Kondoh, H. Uyama, *Chem. Commun.* **2011**, 7422.
[20] C. T. Nguyen, D.-P. Kim, *J. Mater. Chem.* **2011**, *21*, 14226.
[21] C.-G. Wu, T. Bein, *Science* **1994**, *266*, 1013.
[22] S. A. Johnson, P. J. Ollivier, T. E. Mallouk, *Science* **1999**, *283*, 963.
[23] D. Zhao, D. Yuan, H.-C. Zhou, *Energy Environ. Sci.* **2008**, *1*, 222.
[24] W. Lu, D. Yuan, D. Zhao, C. I. Schilling, O. Plietzsch, T. Muller, S. Brase, J. Guenther, J. Blumel, R. Krishna, Z. Li, H.-C. Zhou, *Chem. Mater.* **2010**, *22*, 5964.
[25] D. Yuan, W. Lu, D. Zhao, H.-C. Zhou, *Adv. Mater.* **2011**, *23*, 3723.
[26] A. Lu, A. Kiefer, W. Schmidt, F. Schuth, *Chem. Mater.* **2004**, *16*, 100.
[27] M. Kruk, B. Dufour, E. B. Celer, T. Kowalewski, M. Jaroniec, K. Matyjaszewski, *J. Phys. Chem. B* **2005**, *109*, 9216.
[28] Y. Wang, C. Zhang, S. Kang, B. Li, Y. Wang, L. Wang, X. Li, *J. Mater. Chem.* **2011**, *21*, 14420.
[29] M. Kruk, B. Dufour, E. B. Celer, T. Kowalewski, M. Jaroniec, K. Matyjaszewski, *Chem. Mater.* **2006**, *18*, 1417.
[30] M. Kruk, B. Dufour, E. B. Celer, T. Kowalewski, M. Jaroniec, K. Matyjaszewski, *Macromolecules* **2008**, *41*, 8584.
[31] D. Wu, C. M. Hui, H. Dong, J. Pietrasik, H. J. Ryu, Z. Li, M. Zhong, H. He, E. K. Kim, M. Jaroniec, T. Kowalewski, K. Matyjaszewski, *Macromolecules* **2011**, *44*, 5846.
[32] M. Save, G. Granvorka, J. Bernard, B. Charleux, C. Boissiere, D. Grosso, C. Sanchez, *Macromol. Rapid Commun.* **2006**, *27*, 393.
[33] Z. Zhou, S. Zhu, D. Zhang, *J. Mater. Chem.* **2007**, *17*, 2428.
[34] F. Audouin, H. Blas, P. Pasetto, P. Beaunier, C. Boissiere, C. Sanchez, M. Save, B. Charleux, *Macromol. Rapid Commun.* **2008**, *29*, 914.
[35] P. Pasetto, H. Blas, F. Audouin, C. Boissiere, C. Sanchez, M. Save, B. Charleux, *Macromolecules* **2009**, *42*, 5983.
[36] H. Blas, M. Save, C. Boissiere, C. Sanchez, B. Charleux, *Macromolecules* **2011**, *44*, 2577.
[37] P. Sozzani, S. Bracco, A. Comotti, R. Simonutti, P. Valsesia, Y. Sakamoto, O. Terasaki, *Nat. Mater.* **2006**, *5*, 545.
[38] R. Xing, N. Liu, Y. Liu, H. Wu, Y. Jiang, L. Chen, M. He, P. Wu, *Adv. Funct. Mater.* **2007**, *17*, 2455.
[39] A. C. Sharma, A. S. Borovik, *J. Am. Chem. Soc.* **2000**, *122*, 8946.
[40] M. Hajj-Hassan, S.-J. Kim, M. C. Cheung, L. Yao, V. Chodavarapu, A. Cartwright, *J. Nanophotonics* **2010**, *4*, 043513.
[41] E. Geraud, M. Bouhent, Z. Derriche, F. Leroux, V. Prevot, C. Forano, *J. Phys. Chem. Sol.* **2007**, *68*, 818.
[42] I. Muylaert, M. Borgers, E. Bruneel, J. Schaubroeck, F. Verpoort, P. Van Der Voort, *Chem. Commun.* **2008**, 4475.
[43] C. Feng, H. Li, Y. Wan, *J. Nanosci. Nanotechnol.* **2009**, *9*, 1558.
[44] Z. Yang, J. Wang, K. Huang, J. Ma, Z. Yang, Y. Lu, *Macromol. Rapid Commun.* **2008**, *29*, 442.
[45] S. Huh, J. W. Wiench, J.-C. Yoo, M. Pruski, V. S.-Y. Lin, *Chem. Mater.* **2003**, *15*, 4247.
[46] B. Marler, U. Oberhagemann, S. Vortmann, H. Gies, *Microporous Mater.* **1996**, *6*, 375.
[47] T. K. Mandal, M. S. Fleming, D. R. Walt, *Chem. Mater.* **2000**, *12*, 3481.
[48] K. Kamata, Y. Lu, Y. Xia, *J. Am. Chem. Soc.* **2003**, *125*, 2384.
[49] K. Matyjaszewski, P. J. Miller, N. Shukla, B. Immaraporn, A. Gelman, B. B. Luokala, T. M. Siclovan, G. Kickelbick, T. Vallant, H. Hoffmann, T. Pakula, *Macromolecules* **1999**, *32*, 8716.
[50] W.-H. Zhang, J.-L. Shi, H.-R. Chen, Z.-L. Hua, D.-S. Yan, *Chem. Mater.* **2001**, *13*, 648.
[51] J. Y. Kim, S. B. Yoon, F. Kooli, J.-S. Yu, *J. Mater. Chem.* **2001**, *11*, 2912.
[52] K. Babu, R. Dhamodharan, *Nanoscale Res. Lett.* **2009**, *4*, 1090.
[53] Z. Li, M. C. Johnson, M. Sun, E. T. Ryan, D. J. Earl, W. Maichen, J. I. Martin, S. Li, C. M. Lew, J. Wang, M. W. Deem, M. E. Davis, Y. Yan, *Angew. Chem. Int. Ed.* **2006**, *45*, 6329.
[54] C. Shao, X. Wang, J. Xu, J. Zhao, Q. Zhang, Y. Hu, *J. Org. Chem.* **2010**, *75*, 7002.
[55] A. Bozkurt, W. H. Meyer, J. Gutmann, G. Wegner, *Solid State Ionics* **2003**, *164*, 169.
[56] H. Bayrak, A. Demirbas, N. Demirbas, S. A. Karaoglu, *Eur. J. Med. Chem.* **2010**, *45*, 4726.
[57] L. Kelepouris, G. J. Blanchard, *J. Phys. Chem. B* **2003**, *107*, 1079.
[58] B. Sasmaz, G. Baydemir, N. Bereli, S. Senel, H. Yavuz, *Hacettepe J. Biol. Chem.* **2008**, *36*, 47.
[59] M. Furlan, B. A. Perret, E. A. Beck, *Anal. Biochem.* **1979**, *96*, 208.
[60] D. S. Achilias, *Eur. Polym. J.* **2007**, *43*, 2564.
[61] S. Manna, T. Ghoshal, S. K. De, *J. Phys. D: Appl. Phys.* **2010**, *43*, 295403.